

# **Structural Studies of the Palladium-Hydrogen System**

A Thesis submitted for the Degree of  
Doctor of Philosophy

By

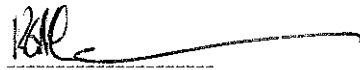
Keith Gordon McLennan

School of Science  
Griffith University

August 2005

## Statement

The thesis herein contains no material which has been submitted for a degree or diploma in any university, and to the best of my knowledge contains no material previously published or written by another person, except where due acknowledgment is made.

A handwritten signature in black ink, appearing to read 'K. McLennan', followed by a long horizontal flourish.

Keith McLennan

## Acknowledgements

Without whom, etc

The work in this thesis was begun in January 2000, and in the intervening five and half years I have received much help from colleagues, family and friends. I am convinced that completion of this thesis would have been much more difficult, if not impossible, without this help and so I set about now to thank them all.

I wish to thank my principal supervisor Associate Professor Evan Gray for guidance and help in all aspects of this work. Evan has taught me much about experimental methods and has provided good council over the years. He also has a good nose for restaurants, a much needed diversion in the middle of experimental runs.

Professor John Dobson, my co-supervisor, provided help with the Density Functional Theory parts, especially in organising access to computer resources.

I would like to thank both Evan and John for organizing a Griffith University School of Science Postgraduate Scholarship near the end of my tenure when it was much needed

My colleagues Dr Tomasz Blach and Dr Mark Pitt have both been a great help to me when preparing for experiments, especially early on during my transformation from theoretician to experimenter. They have also provided much-needed company during those long beam-time runs. Thanks specifically to Tom for showing me the fine art of “power sight-seeing”, and to Mark for introducing the operation of the Rietica computer program to me

During the course of this research, I held an Australian Postgraduate Research award, supplemented with an Australian Institute of Nuclear Science and Engineering award. I wish to thank my AINSE co-supervisor Dr Shane Howard for insightful help into some of the subtleties of Rietveld refinement. I thank AINSE for the financial support and for providing access to the HIFAR diffraction instruments.

In-situ diffraction studies are difficult experiments to perform successfully, and I need to thank all of the instrument scientists who have helped me complete mine. They are, in no particular order, Dr Brett Hunter and Dr Andrew Studer of the Bragg Institute at ANSTO, Dr Peter Fischer (retired) of the SINQ facility at the Paul Scherrer Institute and Kevin Knight of the ISIS facility at the Rutherford Appleton Laboratory. All of these

### III

gentlemen have provided highly professional support during various experiments and their help was invaluable.

I would like to thank both Dr Etich Kisi and Dr Klaus Yvon for helping to improve my understanding of crystallography

Dr Chris Brown was very helpful in providing computer resources when they were most needed.

Finally, I need to thank my partner, Julie, and daughter, Lydia, for so much patience over the last few years. They have put up with my distractions, workload and many absences with good grace and courage. This thesis is dedicated to them.

## Abstract

In this work the palladium-hydrogen system has been studied using experimental and computational techniques. The experimental technique used was in-situ neutron powder diffraction. The in-situ methodology, in which diffraction data are collected from a sample loaded to a known hydrogen concentration, provides an independent measure of the hydrogen occupation of interstitial lattice sites.

Theoretical modeling with the ADF-BAND software was done to calculate lattice parameters and investigate interstitial occupancy

An important driver for this work was a new report of occupation of tetrahedral interstices near the thermodynamic critical temperature, above which the hydriding phase transformation is continuous. The two-pronged approach was adopted to provide experimental input to the modeling and theoretical understanding of the experiments.

The focus of the work carried out was the peri-critical region of the palladium-hydrogen system. While raising significant technical challenges to the experiments, this meant that modeling was made easier, as the system is single-phase above the critical temperature. Fairly direct comparisons of theory and experiment were therefore possible.

The experiments performed have revealed much new information about the previously well studied palladium-hydrogen system. Differences have been identified in some thermodynamic properties of this system based upon the bulk form of the palladium, whether solid sheet or finely divided. The two forms have different shapes to their pressure-composition isotherms, the form of the hysteresis is different and they display markedly different thermodynamic critical temperatures.

The determination of the thermodynamic critical temperature was also focused on. The classical method of determining critical temperature by the disappearance of the hysteresis in the pressure-composition-temperature (p-c-T) curves has proved to be inaccurate. Above the critical temperature, but still in the peri-critical region, where the hysteresis in the p-c-T curves proves undetectable, it is possible to distinguish two phases via diffraction pattern refinement. The nature of these phases is slightly different to the typical  $\alpha$  and  $\beta$  phases located well below the critical temperature where the phases behave very differently. In the peri-critical region the two phases are very similar and each follows the Vegard relationship independently.

A significant part of the research was directed at the location of deuterium atoms in the palladium face centered cubic (FCC) lattice. Two sites in the FCC lattice are available to the deuterium, the tetrahedral site and the octahedral site, and traditionally it is thought that only the octahedral site is occupied. Based on fundamental calculations on peak heights, as well as on full Rietveld refinement, it has been shown that there is now compelling evidence for tetrahedral occupation in the peri-critical region of palladium-deuterium

The theoretical calculations performed accurately estimated the lattice parameters for the range of palladium-hydrogen stoichiometries. By enlarging the modeled unit cell, several hydrogen concentrations could be represented. These calculations provided support for the idea of tetrahedral site occupation by hydrogen of the palladium FCC lattice, and predicted the experimentally observed trend to higher tetrahedral occupancy in the middle of the concentration range Pd to PdH.

## Table of Contents

Statement	I
Acknowledgements	II
Abstract	IV
Table of Contents	VI
List of Figures	XI

### Chapter One      Thesis Overview

1.1 The Hydrogen Economy	2
1.2 The Problem of Hydrogen Storage	3
1.3 The Study of Palladium-Hydrogen	4
1.4 Thesis Structure	5
References	7

### Chapter Two      Materials and Methods

2.1 Introduction	9
2.2 Palladium	9
2.3 Hydrogen	10
2.4 Palladium-Hydrogen System	10
2.4.1 Characteristics of the Palladium Hydrogen System	11
2.4.2 The Palladium-Hydrogen Phase Diagram	11
2.4.3 The Palladium-Hydrogen Critical Temperature	12
2.4.4 Palladium and the Storage of Hydrogen	13
2.4.5 Palladium and the Separation of Hydrogen	14
2.5 Methods for Determining Hydrogen-to-Metal Ratios	15
2.5.1 The Gravimetric Technique	16

2.5.2	The Sieverts Technique	16
2.5.3	The Compressibility of Deuterium	19
2.5.4	The Hot-Cold Volume Model	21
2.6	Neutron-Beam Diffraction Instruments	22
2.6.1	The HIFAR MRPD Instrument	23
2.6.2	The HIFAR HRPD Instrument	23
2.6.3	The SINQ HRPT Instrument	25
2.6.4	The ISIS HRPD Instrument	26
2.7	Density Functional Theory	27
	References	28

### **Chapter Three      In-situ Neutron-beam Diffraction Studies of the Palladium-Deuterium System: Macroscopic Properties**

3.1	Introduction	31
3.2	Sample Preparation	31
3.3	HIFAR MRPD October 2001	33
3.3.1	Manometrics: Supercritical Isotherm	34
3.3.2	Manometrics: Critical Isotherm	35
3.3.3	Manometrics: Subcritical Isotherm	37
3.3.4	The Peri-critical Region of the Palladium-Deuterium System	38
3.4	SINQ HRPT May 2002	39
3.4.1	Manometrics	39
3.5	HIFAR MRPD July 2002	41
3.5.1	Manometrics	41
3.5.2	Instrument Calibration Problems	42



## VIII

3.6 HIFAR HRPD October 2003	44
3.6.1 Manometrics	44
3.7 ISIS HRPD March/April 2004	46
3.7.1 Issues Affecting the Proposed Beam-Time	46
3.7.2 Manometrics	47
3.7.3 The Pre-Dislocation 310°C Isotherm	52
3.7.4 The 120°C Isotherm	53
3.7.5 The Annealing Temperature Scans	54
3.7.6 The Post-Annealing 310°C Isotherm and Quench	55
3.8 Conclusions and Discussion	57
References	59

## **Chapter Four      In-situ Neutron-beam Diffraction Studies of the Palladium-Deuterium System: Lattice Parameters**

4.1 Introduction	62
4.2 Rietveld Analysis	64
4.3 HIFAR MRPD October 2001	65
4.3.1 Introduction	65
4.3.2 Refinement Problems	65
4.3.3 The Super-Critical Isotherm	65
4.3.4 The Critical Isotherm	67
4.3.5 The Sub-Critical Isotherm	68
4.3.6 The Peri-Critical Region Lattice Parameters	69
4.4 SINQ HRPT May 2002	70
4.4.1 Introduction	70
4.4.2 Lattice Parameters	70

4.5	HIFAR HRPD July 2002	71
4.5.1	Introduction	71
4.5.2	Refinement Problems	71
4.5.3	Lattice Parameters	71
4.6	HIFAR HRPD October 2003	73
4.7	ISIS HRPD March/April 2004	74
4.7.1	Introduction	74
4.7.2	The Lattice Parameters of the Pre-Dislocation 310°C Isotherm	75
4.7.3	The Lattice Parameters of the 120°C Isotherm	76
4.7.4	The Annealing Temperature Scan Patterns	77
4.7.5	The Post-Annealing Lattice Parameters	82
4.7.6	All ISIS HRPD Results	83
4.8	Comparison of All Results	84
4.9	Conclusions and Discussions	85
	References	89

## Chapter Five      In-situ Neutron-beam Diffraction Studies of the Palladium-Deuterium System: Deuterium Occupation of the Tetrahedral Site

5.1	Introduction	91
5.2	Structure Factor Rules Governing the Octahedral and Tetrahedral Site Occupation of the FCC Lattice	93
5.3	A Comparison of the Calculated Peak Heights and the Experimentally Measured Peak Heights	102
5.4	Procedure for Analysing High Resolution Data	108
5.5	Refined Occupations	109
5.6	Conclusions and Discussions	113
	References	115

**Chapter Six                      A Computational Study of the Peri-Critical Region of  
the Palladium-Hydride System Using Density  
Functional Theory Techniques**

6.1 Introduction	117
6.1.1 Density Functional Theory	118
6.1.2 The Hartree Approximation	118
6.1.3 Exchange and Correlation	119
6.2 Theory of ADF-BAND	119
6.3 Computational Technique	121
6.3.1 Unit Cells Used for Computations	122
6.3.2 Orbital Functions	125
6.4 Calculated Lattice Parameters	129
6.5 Octahedral and Tetrahedral Site Occupation	131
6.5.1 General Palladium-Hydrogen System Calculations	131
6.5.2 Detailed Calculations of $\text{Pd}_8\text{H}_3$	134
6.5.3 Energy Profile of the Cube Diagonals	136
6.6 Conclusions and Discussions	140
References	142
<b>Summary</b>	<b>143</b>
<b>References</b>	
<b>Appendix                      Published Works</b>	<b>A-I</b>
<i>Prediction of Dispersion Forces: Is There a Problem?</i>	
<i>An Equation of State for Deuterium gas to 1000 bar</i>	
<i>Soft Cohesive Forces</i>	

## List of Figures

Fig 2.1	The face-centered-cubic crystal structure	9
Fig 2.2	Palladium-protium p-c-T relationships and the palladium-protium phase diagram	12
Fig 2.3	Schematic of hydrogen separation in a palladium membrane	15
Fig 2.4	Experimental setup of an in-situ diffraction study	facing 16
Fig 2.5	The HRPD diffractometer	24
Fig 2.6	SINQ HRPT sample table	25
Fig 2.7	SINQ HRPT schematic	25
Fig 2.8	ISIS facility at RAL	26
Fig 3.1	Schematic of Sieverts apparatus used in October 2001	33
Fig 3.2	Pd-D Supercritical isotherm	35
Fig 3.3	Pd-D Supercritical diffraction patterns	35
Fig 3.4	Pd-D Critical isotherm	36
Fig 3.5	Pd-D Critical diffraction patterns	36
Fig 3.6	Pd-D Sub-critical isotherm	37
Fig 3.7	Pd-D Sub-critical diffraction patterns	37
Fig 3.8	The peri-critical region of palladium-deuterium	38
Fig 3.9	Pressure-composition isotherms for the palladium-deuterium bulk sheet sample	facing 39
Fig 3.10	Schematic of Sieverts apparatus used in May 2002 on SINQ HRPT	39

Fig 3 11 Neutron diffraction patterns from palladium-deuterium	40
Fig 3 12 Schematic of Sieverts apparatus used in July 2002 on HIFAR MRPD	41
Fig 3 13 Room temperature p-c-T diagram for palladium- deuterium	42
Fig 3 14 Room temperature neutron diffraction patterns of palladium-deuterium	42
Fig 3 15 Detail of diffraction patterns of palladium-deuterium collected on HIFAR MRPD July 2002	43
Fig 3 16 Schematic of Sieverts apparatus used on HIFAR HRPD October 2003	44
Fig 3 17 p-c-T diagram for palladium-deuterium	45
Fig 3 18 Diffraction patterns collected for palladium-deuterium on HIFAR HRPD October 2003	45
Fig 3 19 Schematic of Sieverts apparatus used on ISIS HRPD May 2004	47
Fig 3 20 Pressure-composition-temperature graph of palladium- deuterium	48
Fig 3 21 Palladium-deuterium isotherms	facing 49
Fig 3 22 Neutron-beam diffraction patterns from palladium collected on ISIS HRPD	51
Fig 3 23 Palladium-deuterium isotherm at 310°C	52
Fig 3 24 Palladium-deuterium neutron diffraction patterns for 310°C isotherm collected on ISIS HRPD	52
Fig 3 25 Palladium-deuterium isotherm at 120°C	53

Fig 3.26 Palladium-deuterium neutron diffraction patterns collected ISIS HRPD, sample at 120°C	53
Fig 3.27 Palladium annealing temperature neutron diffraction patterns ISIS HRPD	55
Fig 3.28 Palladium annealing temperature neutron diffraction patterns ISIS HRPD (detail)	55
Fig 3.29 Palladium-deuterium 310°C isotherm and quench step	56
Fig 3.30 Palladium-deuterium neutron diffraction patterns collected ISIS HRPD	56
Fig 4.1 Supercritical isotherm (300°C), refined lattice parameter vs. deuterium content, absorption isotherm only	66
Fig 4.2 Critical isotherm (280°C), refined lattice parameter vs. deuterium content, absorption and desorption isotherms	67
Fig 4.3 Sub-critical isotherm (250°C), refined lattice parameter vs. deuterium content, absorption and desorption isotherms	68
Fig 4.4 Lattice parameters of the palladium-deuterium system near the peri-critical region	facing 69
Fig 4.5 Refined lattice parameters vs. deuterium concentration at 295-320°C	facing 70
Fig 4.6 Refined lattice parameters from room-temperature palladium-deuterium	facing 71
Fig 4.7 Comparison of lattice parameters refined from experiments of October 2001 and July 2002	72
Fig 4.8 Refined lattice parameters of palladium-deuterium on HRPD HIFAR October 2003	73
Fig 4.9 Refined palladium-deuterium lattice parameters for 310°C isotherm	75

Fig 4.10 Refined lattice parameters from the 120°C isotherm	facing 76
Fig 4.11 Critical and sub-critical lattice parameters	77
Fig 4.12 Annealing temperature lattice parameters	78
Fig 4.13 All pure palladium lattice parameters	78
Fig 4.14 Refined thermal parameter B during annealing	79
Fig 4.15 Refined peak-shape parameter $\gamma_1$ during annealing	79
Fig 4.16 Refined peak-shape parameter $\gamma_2$ during annealing	80
Fig 4.17 Refined particle size parameter $A_{size}$ during annealing	80
Fig 4.18 Palladium-deuterium annealing experiment peak-shape parameters	81
Fig 4.19 Lattice parameters of the palladium-deuterium 310°C isotherm and quench	82
Fig 4.20 All results from ISIS HRPD March/April 2004	83
Fig 4.21 The lattice parameters of $PdH_x$ and $PdD_x$ from neutron diffraction studies	84
Fig 5.1 Location of the tetrahedral and octahedral sites in the face centered cubic structure	91
Fig 5.2 Palladium deuterium calculated peak heights of the three lowest order peaks on a time-of-flight neutron diffractometer using an octahedral occupation only model	facing 103
Fig 5.3 Palladium deuterium relative peak heights of the three lowest order peaks for a time-of-flight neutron diffractometer using an octahedral occupation only model	104
Fig 5.4 Palladium deuterium relative peak heights of the three lowest order peaks for a constant-wavelength neutron diffractometer using an octahedral occupation only model	104

Fig 5.5	Relative peak height comparisons for a time-of flight neutron diffractometer, expected and experimental	105
Fig 5.6	Relative peak height comparisons for a constant wavelength neutron diffractometer, expected and experimental	106
Fig 5.7	Relative peak height comparisons for a constant-wavelength neutron diffractometer, expected and experimental	107
Fig 5.8	Palladium-deuterium system. Deuterium octahedral site and tetrahedral site occupation numbers near the system critical temperature.	110
Fig 5.9	Palladium-deuterium system Single-phase deuterium octahedral and tetrahedral site occupation numbers at 310°C	111
Fig 5.10	Thermal parameters of octahedral and tetrahedral located deuterium in palladium at 310°C	112
Fig 6.1	Primitive basis set for generating FCC structure. Single atom basis with rhombohedral translation axes	122
Fig 6.2	Cubic basis for generating the FCC structure Four atom basis with cubic translation axes	123
Fig 6.3	Double-cubic basis set for generating FCC structure. Eight atom basis with rectilinear translation axes	124
Fig 6.4	Calculated lattice parameters for $\text{Pd}_x\text{H}$	129
Fig 6.5	Calculated lattice parameters for $\text{Pd}_x\text{H}$ compared to experimental results from this thesis	130
Fig 6.6	Palladium Hydride Energy of Formation - effect of moving hydrogen atoms from octahedral to tetrahedral sites	131



Fig 6 7 Palladium Hydride Fermi Energy - effect of moving hydrogen atoms from octahedral to tetrahedral sites	133
Fig 6 8 Pd <sub>8</sub> H <sub>3</sub> Energy of Formation – octahedral/tetrahedral site occupation comparison	134
Fig 6.9 Nearest neighbour considerations for 8-atom rectilinear “double-cubic” unit cell	136
Fig 6 10 Energy of Formation Pd <sub>2</sub> H	facing 137
Fig 6 11 Fermi Energy Pd <sub>2</sub> H	facing 137
Fig 6.12 Energy of Formation Pd <sub>2</sub> H	facing 137
Fig 6.13 Fermi Energy Pd <sub>2</sub> H	facing 137
Fig 6 14 Energy of Formation Pd <sub>2</sub> H – low symmetry configuration	138
Fig 6.15 Energy of Formation Pd <sub>4</sub> H	facing 139
Fig 6.16 Fermi Energy Pd <sub>4</sub> H	facing 139
Fig 6 17 Energy of Formation Pd <sub>4</sub> H	facing 139
Fig 6.18 Fermi Energy Pd <sub>4</sub> H	facing 139

## **Chapter One**

### **Thesis Overview**

- 1.1 The Hydrogen Economy
- 1.2 Problems of Hydrogen Storage
- 1.3 The Study of Palladium-Hydrogen
- 1.4 Thesis Structure

References

## Chapter One

### Thesis Overview

#### 1.1 The Hydrogen Economy

History displays humanity's constantly increasing demand upon the environment, through both the depletion of resources and the emission of pollutants, from a constantly increasing population needing increased mobility

The modern world needs clean, safe, efficient, renewable energy vectors (carriers). Hydrogen has many advantages as an energy vector [1, 2]. The *Hydrogen Economy* refers to a group of energy technologies that use a hydrogen vector to store and distribute energy. It is thought that the Hydrogen Economy will be able to provide an alternative to humanities non-renewable, polluting fossil fuel based economy.

Hydrogen is the most abundant element in the universe, accounting for around 75% by species. It exists naturally as a low-density diatomic molecule,  $H_2$ , which burns with oxygen to produce water,  $H_2O$ , releasing 121 kJ of energy per gram of  $H_2$ . If burnt in air, traces of nitrogen oxides will also be produced.

Table 1.1 compares some physical properties, relevant to use as a fuel, of hydrogen against natural gas and gasoline. At a given pressure, hydrogen has about one-third the energy as the same volume of methane. As a liquid, it has about one-third the volumetric energy density as gasoline. For reasonable onboard storage volumes, hydrogen must be either compressed to high pressure (hundreds of bar) or liquefied (at around 20 K). Hydrogen does have the highest heating value per kilogram of any fuel, making it attractive as a mobile application fuel source.

Hydrogen can be used for combustion in internal combustion engines with approximately 25% overall efficiency. Hydrogen can also be used for "combustion" in a fuel cell, which avoids the Carnot cycle and delivers 50 - 60% efficiency. It is already being used successfully as an onboard rocket fuel.

Hydrogen does have some issues in being such a small, low-density gas compared to the two other fuels in Table 1.1. It is more prone to leaks, though will disperse faster. Its higher flame velocity in air is a disadvantage in an explosive situation. Its larger range of flammability and detonability limits also makes it more dangerous if leaking hydrogen is

allowed to build up in an enclosed space, though allows more flexibility in its use as a fuel. Hydrogen can diffuse into metals and cause embrittlement in a range of steels, which is an issue when choosing storage container construction material. This ability to diffuse through certain metals can be exploited as a method to get hydrogen, and also presents a possible solution to the onboard storage problem.

<b>Table 1.1: Physical Properties of Hydrogen, Methane, and Gasoline[2]</b>			
	Hydrogen	Methane	Gasoline
Molecular weight ( $\text{g mol}^{-1}$ )	2.016	16.04	~ 110
Mass density ( $\text{kgN}_2^{-1}\text{m}^{-3}$ ) at P=0.101 MPa, T=0°C	0.09	0.72	720-780 (liquid)
Mass density of liquid H <sub>2</sub> at 20 K ( $\text{kgN}_2^{-1}\text{m}^{-3}$ )	70.9	—	—
Boiling Point (K)	20.2	11.6	310-478
Higher heating value ( $\text{MJkg}^{-1}$ ) (assumes water is produced)	142.0	55.5	47.3
Lower heating value ( $\text{MJkg}^{-1}$ ) (assumes steam is produced)	120.0	50.0	44.0
Flammability limits (% volume)	4.0-75.0	5.3-15.0	1.0-7.6
Detonability limits (% volume)	18.3-59.0	6.3-13.5	1.1-3.3
Diffusion velocity in air ( $\text{ms}^{-1}$ )	2.0	0.51	0.17
Buoyant velocity in air ( $\text{ms}^{-1}$ )	1.2-9.0	0.8-6.0	Non-buoyant
Ignition energy (mJ)			
At stoichiometric mixture	0.02	0.29	0.24
At lower flammability limit	10	20	n.a.
Flame velocity in air ( $\text{cms}^{-1}$ )	265-325	37-45	37-43
Toxicity	Nontoxic	Nontoxic	Toxic > 50 ppm

## 1.2 The Problem of Hydrogen Storage

The major problem facing the adoption of hydrogen for mobile applications is that of onboard storage. A viable onboard fuel storage system must be compact, lightweight, cheap, rugged, easily and rapidly refillable and safe. It must also be capable of storing enough hydrogen to provide a reasonable traveling range, and must retain stored hydrogen for a long time without leakage.

The only way of using conventional storage methods to obtain sufficiently high mass energy densities with hydrogen is to store it under very high pressure, or as a cryogenic liquid. In either case, the storage container is much bulkier than for liquid fuels or for natural gas, because it must be reinforced to contain the pressurized gas, or it must incorporate refrigeration equipment. The ability of certain metals and other solid materials to absorb hydrogen into their bulk is seen as one method of overcoming this storage problem, but only if a light enough material can be found which absorbs hydrogen at a sufficient energy density. The U S Department of Energy sets a lower limit of 6.5-wt% hydrogen to container ratio for a viable mobile hydrogen storage system.

### 1.3 The Study of Palladium-Hydrogen

There are a number of likely candidates for such a storage material. Palladium, the oldest known metal able to form a hydride, is certainly *not* one of them, owing to its high atomic weight and very high cost.

However, the palladium-hydrogen system is probably the simplest metal-hydrogen system, and is a valuable model for investigating some of the most fundamental problems associated with hydrogen adsorption by metals. Palladium and palladium-hydrogen are historically well categorized, easy to study via diffraction techniques, and simple enough to model theoretically using moderate processing power. This thesis addresses a number of fundamental issues associated with metal-hydrogen systems in the palladium-hydrogen context, including the nature of the thermodynamic critical point, the relationship between lattice parameter and hydrogen-to-palladium concentration, and the particular sites in the palladium crystal lattice that are preferentially occupied by hydrogen. In particular, the possible occupancy of hydrogen sites in close proximity is interesting from the point of view of high hydrogen density and is a focal point of this thesis.

There has been no thorough study of the region around the palladium-hydrogen critical temperature ( $T_c$ ). This is scientifically interesting, as it marks the point where the possibility of the existence of two phases disappears, and is also convenient for studying the effects of varying hydrogen occupancy in a continuous range of hydrogen concentrations above  $T_c$ .

There are two sites in the palladium face-centered-cubic crystal structure which hydrogen atoms in palladium-hydrogen can occupy, the octahedral site and the tetrahedral site. The generally accepted view is that hydrogen atoms occupy the octahedral sites, and are transient in the tetrahedral sites, which lie on the diffusion path between octahedral sites. There are twice as many tetrahedral sites available as octahedral sites, so preferential occupation of the tetrahedral sites could conceivably double palladium's storage capacity. Diffusion of hydrogen through palladium is known to occur via interstitial hopping between octahedral sites *via* tetrahedral sites. A fundamental understanding of the nature of the occupation of such *transient* sites is seen as a basic step towards possible storage and permittivity improvements in all metal-hydrogen alloys.

#### 1.4 Thesis Structure

The thesis is based on four neutron-beam *in-situ* diffraction studies of the palladium-deuterium system, and a Density Functional Theory based computational study of Palladium-Hydrogen

Chapter 1 introduces the context of the thesis

Chapter 2 is a discussion of the materials used in the experimental parts, palladium and hydrogen, and their interaction. The techniques used during the study are discussed, including the nature of palladium-hydrogen pressure-composition-temperature curves and the Sieverts method of determining them. A new formula for the compressibility of deuterium, developed during the course of this study, is introduced.

Chapter 3 describes in detail the manometry involved in the palladium-hydrogen isotherms, and discusses the collection of the diffraction patterns and some of their obvious features.

Chapter 4 examines the lattice parameter data extracted from the diffraction patterns, via Rietveld analysis, in relation to Vegard's Law. Other refined values are discussed, as is the nature of the thermodynamic critical temperature of palladium-deuterium.

Chapter 5 analyses the diffraction patterns specifically as to the issue of occupation of the tetrahedral sites in the palladium FCC structure by deuterium atoms. This is done by

Careful refining of the three lowest order FCC peaks ([111], [200], [220]) specifically against the amount of deuterium in either the octahedral or the tetrahedral FCC sites.

Chapter 6 presents the result of the Density Functional Theory (DFT) study of the palladium-hydrogen system. The lattice parameters corresponding to the range of hydrogen-to-palladium ratios from pure palladium up to stoichiometric PdH are calculated through pseudo-multi point calculations and minimization of the total energy function. There is some general investigation of the issue of octahedral and tetrahedral site occupation across all stoichiometries and a detailed investigation in a few specific palladium-hydrogen configurations.

Chapter 7 summarizes the conclusions of each chapter and suggests further work.

Appendix: Published Papers

1. Gray, E M , Unpublished, 1991.
2. Ogden, J.M , Physics Today, 2002 **April 2002**: p 69-75



## **Chapter Two**

### **Materials and Methods**

#### 2.1 Introduction

#### 2.2 Palladium

#### 2.3 Hydrogen

#### 2.4 Palladium-Hydrogen System

##### 2.4.1 Characteristics of the Palladium Hydrogen System

##### 2.4.2 The Palladium-Hydrogen Phase Diagram

##### 2.4.3 The Palladium-Hydrogen Critical Temperature

##### 2.4.4 Palladium and the Storage of Hydrogen

##### 2.4.5 Palladium and the Separation of Hydrogen

#### 2.5 Methods for Determining Hydrogen-to-Metal Ratios

##### 2.5.1 The Gravimetric Technique

##### 2.5.2 The Sieverts Technique

##### 2.5.3 The Compressibility of Deuterium

##### 2.5.4 The Hot-Cold Volume Model

#### 2.6 Neutron-Beam Diffraction Instruments

##### 2.6.1 The HIFAR MRPD Instrument

##### 2.6.2 The HIFAR HRPD Instrument

##### 2.6.3 The SINQ HRPI Instrument

##### 2.6.4 The ISIS HRPD Instrument

#### 2.7 Density Functional Theory

#### References

## Chapter Two

### Materials and Methods

#### 2.1 Introduction

In the following chapter the fundamental science behind the materials and experimental techniques used throughout this thesis will be explained.

#### 2.2 Palladium

Palladium, chemical symbol Pd, is a Group 10 (Platinum Group), 4d transition metal, with atomic number 46 and atomic mass 106.42(1). It has an electronic configuration of  $[\text{Kr}] 4d^{10}$  and a shell structure 2 8 18 18 0. Its crystal structure is face-centered-cubic (FCC) with space group  $Fm\bar{3}m$  and a lattice parameter of  $3.8907 \text{ \AA}$  (at 0 K). FCC comprises a cubic unit cell with lattice points on the corners and in the centre of each face, as shown in fig 2.1

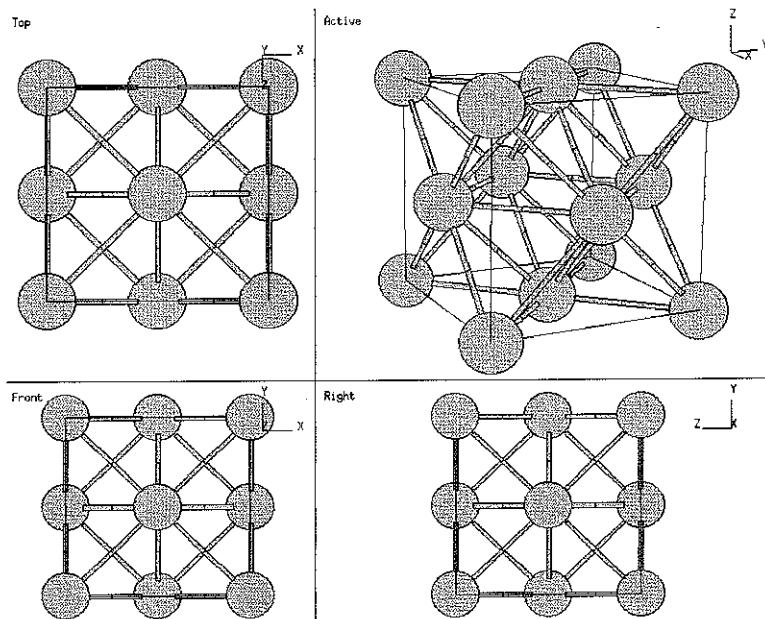


Fig 2.1 The face-centered-cubic crystal structure.

Palladium has a co-efficient of linear thermal expansion  $= 11.8 \times 10^{-6} \text{ K}^{-1}$  (at room temperature).

## 2.3 Hydrogen

Hydrogen, chemical symbol H, is the simplest chemical element with an electronic configuration  $1s^1$ . It has atomic number 1 and atomic mass 1.0079(7). Hydrogen has no fully suitable position on the periodic table, and fits equally well in either group 1A (alkali metals) or Group 7A (halogens).

There are three isotopes of hydrogen, namely protium ( $^1_1\text{H}$ ), deuterium ( $^2_1\text{H}$ , symbol D) and tritium ( $^3_1\text{H}$ , symbol T). The natural abundance of the stable hydrogen isotopes are protium, 99.985%; and deuterium, 0.015%. Tritium is a radioactive isotope with a half-life of about 12.5 years.

Unless specifically stated otherwise, a reference in this work to *hydrogen*, will be meant to indicate any of the three isotopes.

## 2.4 Palladium-Hydrogen System

Palladium has a unique feature amongst elements in that it will spontaneously absorb up to 900 times its own volume of hydrogen at standard temperature and pressure (STP), equivalent to about 0.6-wt%. Other transition metals can be forced to absorb hydrogen and in a number of the so formed compounds, palladium included, the ratio of hydrogen atoms to metal atoms is not a constant. Such compounds are called *interstitial hydrides*. The following equations describe the formation of these hydrides.



Hydrogen can be introduced into the palladium bulk from the gaseous phase, or into a palladium cathode by electrolysis from a solution. In the current study the hydrogen was always introduced via the gaseous phase.

### 2.4.1 Characteristics of the Palladium-Hydrogen System

The absorption of hydrogen from the gaseous phase by palladium is characterised by the following steps:

1. Movement of  $H_2$  to the palladium surface
2. Adsorption of  $H_2$  onto the palladium surface
3. Dissociation of  $H_2$  into elemental hydrogen.
4. Loss of two electrons into the metal to form two  $H^+$  ions
5. N-type conduction of the electrons through the bulk metal
6. Diffusion of the protons via interstitial hopping

There are two phases associated with the palladium-hydrogen system. At low hydrogen concentration it forms a randomly dispersed solid solution of hydrogen in the palladium bulk, the so-called *alpha* phase. At higher hydrogen concentrations palladium-hydride is formed, the *beta* phase, characterized by long range ordering of the hydrogen atoms.

Elemental palladium has  $\sim 0.36$  holes in its “4d” conduction band. Each absorbed hydrogen atom contributes some portion of its own electron to the palladium-hydride band structure, and the maximum hydrogen-to-palladium atomic ratio easily obtainable is  $\sim 0.6$ , presumably the point where the “4d” band is filled. Any hydrogen absorbed in excess of this is contributing electrons to the “5s” palladium band. Stoichiometric PdH has the simple-cubic NaCl structure, formed by two interlocking FCC structures, one of palladium and one of hydrogen.

### 2.4.2 The Palladium-Hydrogen Phase Diagram

A locus of points showing the relationship between equilibrium hydrogen vapour pressure and hydrogen content at a constant temperature is called a pressure-concentration-temperature (p-c-T) diagram. Fig 2.2 shows how a collection of p-c-T diagrams over a range of temperatures can be used to construct the palladium-hydrogen (specifically palladium-protium) phase diagram.

The section of the phase diagram in Fig 2.2 beneath the dashed line indicates the conditions necessary for the  $\alpha$ - and  $\beta$ -phases to co-exist.

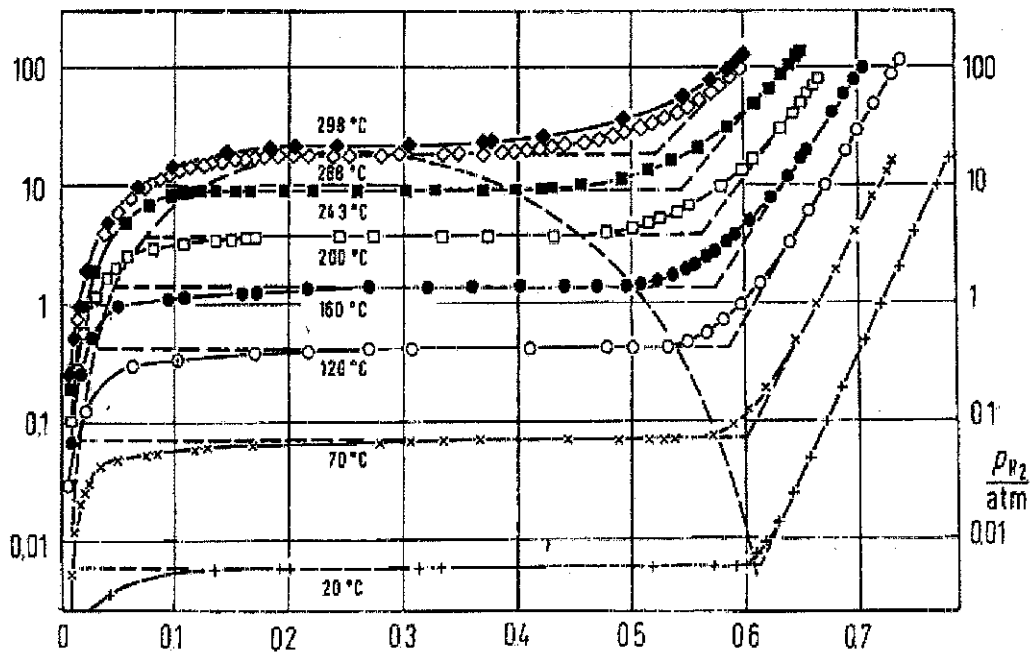


Fig 2.2: Palladium-protium p-c-T relationships and the palladium-protium phase diagram [1]

### 2.4.3 The Palladium-Hydrogen Critical Temperature

The critical temperature ( $T_c$ ) of the palladium hydrogen system is defined as that temperature below which any p-C-T isotherm traverses a two-phase region ( $\alpha$ -phase plus  $\beta$ -phase). A characteristic of any isotherm below the critical temperature is hysteresis between its absorption leg and the desorption leg. Above  $T_c$  the transition from  $\alpha$ -phase to  $\beta$ -phase is a smooth one, and it is generally accepted that the critical temperature and pressure marks the point where the hysteresis disappears. On the hydride phase diagram this is shown as a point of inflection at  $T_c$  and the critical pressure ( $P_c$ ). In Figure 2.2 the critical temperature is shown as 298°C. The relationship between hysteresis and  $T_c$  will be questioned here.

The palladium-hydride phase diagram is directly analogous to the trends in isotherms representing the changes in volume of a real gas as a function of pressure. In the case of compression of gas the critical isotherm corresponds to the temperature boundary dividing the possibility or impossibility of forming a liquid. Above the critical temperature of the PdH system, two solid hydride phases cannot exist together under equilibrium conditions for any hydrogen concentration. Below the critical temperature the  $\alpha$ - and  $\beta$ -phases of the

system can co-exist, represented by the horizontal, pressure invariant, portion of the isotherm.

The two-phase region has always been of particular interest to those involved in the study of metal-hydrides with a view to hydrogen storage. The critical temperature represents the boundary dividing the possibility or impossibility of the formation of a two-phase system. Below this critical temperature a two-phase system exists comprising the low-concentration solid solution ( $\alpha$ -phase) and the high concentration hydride ( $\beta$ -phase), and by exploiting the phase change large amounts of hydrogen can be absorbed or desorbed from the metal with little change in the gas pressure.

The peri-critical region of the palladium-hydride system is of particular interest to the current study as detailed neutron-beam diffraction studies have not been performed here previously. The super-critical region also lends itself well to computational studies (see Chapter 6).

There is some disagreement in the literature about the precise value of the critical temperature for palladium-hydrogen. Much of this disagreement may be due to the differing physical characteristics of the palladium samples used by researchers. Wicke and Blaurock [2] report a critical temperature of  $T_c = 556 \pm 1$  K and  $P_c = 39 \pm 0.5$  bar for palladium-deuterium. This is in marked contrast to that generally reported in the literature of  $T_c = 571$  K for palladium-hydride, especially taking into account that the palladium-deuterium critical temperature should be around  $10^\circ\text{C}$  higher than that for the hydride. Fukai [3] reports the same critical temperature as Wicke and Blaurock. It appears that solid sheet palladium has a different critical temperature than powdered palladium. In this work critical temperatures were evaluated using diffraction to distinguish the two-phase and single-phase regions, giving new insight into this problem.

#### 2.4.4 Palladium and the Storage of Hydrogen

The current United States Department of Energy (US DOE) target for viable hydrogen storage materials is 6.5 wt% i.e. the ratio of weight of fuel stored to the weight of the total storage device must attain at least 6.5%. At stoichiometric PdH the ratio of hydrogen and palladium's atomic weights is 0.95%, and this is an optimistic attainment at non-cryogenic temperatures. Considering that the weight of a storage vessel must also be factored into the

US DOE calculations, it is plain to see that pure palladium is not a viable hydrogen storage material. Palladium is unfortunately also far too expensive to consider as a feasible material for hydrogen storage. Its choice as a study material here is due to its relative simplicity, which makes it ideal as a modeling system and as a tool to understand the metal-hydride interaction.

#### **2.4.5 Palladium and Hydrogen Separation**

The diffusion properties, and high selectivity, of hydrogen by palladium and some of its alloys has been utilized to produce hydrogen separation membranes. A thin metal film of palladium or an alloy is exposed to a mixture of gasses containing hydrogen. The basic driving force for the permeation of hydrogen through such membranes is a concentration gradient. This is enhanced by hydrogen partial pressure differential across the membrane using either vacuum or an inert sweep gas on the outlet side or increasing the feed side pressure. The hydrogen flux is found to be generally proportional to the square root of pressure differential across the membrane.

Schematically the process is shown in Fig. 2.3 and the key process steps are as follows

1. Movement of  $H_2$  to the membrane surface on the feed gas side.
2. Dissociation of  $H_2$  into elemental hydrogen
3. Loss of an electron into the metal to form two  $H^+$  ions
4. N-type conduction across the membrane
5. Diffusion of  $H^+$  ions through bulk of the membrane through interstitial hopping
6. Reacquisition of electron at or near the exhaust side of the membrane
7. Re-association of hydrogen into  $H_2$
8. Movement of  $H_2$  into the exhaust gas stream

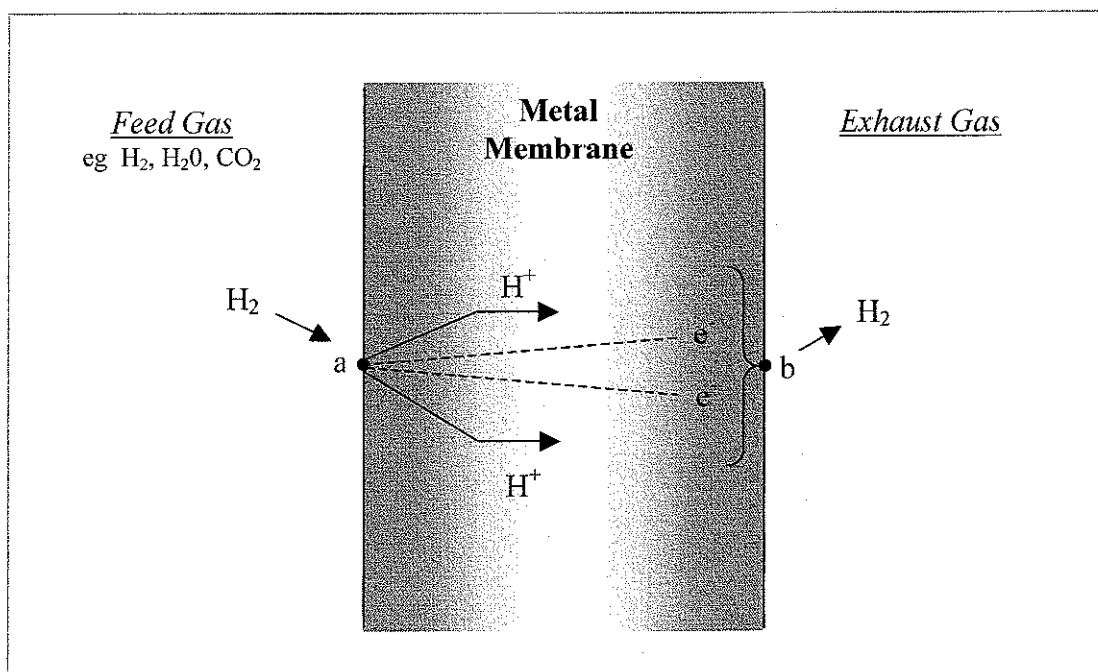


Fig 2 3: Schematic of Hydrogen Separation in a Pd membrane

Currently palladium, and palladium-alloy, membranes have only been used to produce ultra-high purity hydrogen in small quantities for specialist applications e.g. hydrogen for fuel-cells. For higher volume applications palladium becomes unfeasible due to its classification as a critical resource, it is both expensive and currently limited in resource.

## 2.5 Methods for Determining Hydrogen-to-Metal Ratios

Two methods are primarily used to determine the amount of hydrogen sorbed from the gaseous phase during experiments investigating the isotherms of metal-hydrides. Each has advantages and disadvantages.

The *gravimetric* method consists of weighing the sample and its adsorbed hydrogen, but is very sensitive to relatively heavy adsorbed impurities, particularly  $O_2$  and  $H_2O$ . The method of *Sieverts* was used in all experiments described in this thesis for two main reasons: (i) The Sieverts technique is especially suitable for *in-situ* hydrogenation experiments, in which a hydrided sample is formed from the host material and hydrogen gas while collecting data by a suitable microscopic probe technique, neutron diffraction in this case (ii) The Sieverts technique is insensitive to impurities. This results as bulk experimental equipment (e.g. a mass balance) is not required in the sample area.



Note that it has been shown to be possible to obtain neutron diffraction patterns from palladium electrodes, electrochemically loaded with deuterium [4]

### **2.5.1 The Gravimetric Technique**

In the case of experiments involving diffraction studies, the necessity for the presence of bulky mass-balances in the sample area limits the gravimetric method's usefulness against the Sieverts technique, whose only requirement is a pressure-cell connected to remote gas delivery and measurement system

### **2.5.2 The Sieverts Technique**

Figure 2.4 shows a photograph of an experimental setup typical of this study. The sample pressure cell is positioned in a small furnace on the sample table (at the rear of the diffractometer at the center-top of the image). The top of the sample stick is connected via the green-valve to a thin stainless-steel 1/8" tube which leads over the instrument to the hydrogenator on the table at the bottom right of the image, which is conveniently located outside the instrument cage. The hydrogen-to-metal ratio of the sample can be varied and monitored without the experimenter having to enter the instrument area and pass through the safety interlocks. Gravimetric measurements would clearly be impractical in such a situation

Sieverts technique involves establishing a pressure of hydrogen in an accurately known reference volume, admitting this gas to a reaction chamber, and determining the amount absorbed by the sample from the change in the pressure in the system. As the calculation of the quantity of absorbed hydrogen involves taking differences between the amounts of hydrogen gas present before and after absorption, where the absorbed amount may be rather small compared to the amount of gas in the system, it is vital to calculate as accurately as possible the number of moles of gas present under the experimental conditions of temperature and pressure. Thus accurate knowledge of the compressibility,  $Z$ , defined by

$$\frac{pV_m}{RT} = Z \quad (2.2)$$

rather than 1 as in the ideal case, is essential.

The case for all experiments reported here is:

- $n_m$  number of moles of metal (host) atoms in the sample
- $n_s$  number of hydrogen atoms absorbed or desorbed by the sample
- $n_0$  total number of moles of hydrogen atoms in the closed system (constant)
- $n_g$  number of moles of gaseous hydrogen molecules ( $H_2$ ) in the system
- $Z$  compressibility of the hydrogen gas at given temperature and pressure

If the system consists of an arbitrary number of volumes ( $V_i$ ) that are at different temperatures ( $T_i$ ), we can assume that once the reference volume is opened to the sample volume the pressure ( $P$ ) is equal everywhere. Note that in the experiments described in this thesis, there are generally three volumes involved in these calculations, being a *reference volume* ( $V_{ref}$ ) and a sample volume divided into two zones due to partial immersion in a furnace giving a *hot-volume* ( $V_{hot}$  - generally assumed to be at the sample temperature) and a *cold-volume* ( $V_{cold}$  - generally assumed to be at ambient temperature). So generally, the number of moles of hydrogen atoms present is

$$2n_g = \frac{2}{R} P \sum_i \frac{V_i}{Z(P, T_i) T_i} \quad (2.3)$$

In a constant-volume system the pressure is constrained to move on the isochore defined by

$$\frac{2}{R} P \sum_i \frac{V_i}{Z(P, T) T_i} + n_s = n_0 = \text{constant} \quad (2.4)$$

By dividing by the number of moles of sample atoms we get a relationship between the system pressure and the hydrogen-to-sample atomic ratio,

$$\frac{H}{M} = \frac{n_s}{n_m} \quad (2.5)$$

$$P = P_0 - S \frac{H}{M} \quad (2.6)$$

The systems pressure  $P_0$ , immediately after the reference and sample volumes are connected is

$$P_0 = \frac{n_0 R}{2 \sum_i \frac{V_i}{Z_i T_i}} \quad (2.7)$$

and the slope of the isochore is

$$S = \frac{n_m R}{2 \sum_i \frac{V_i}{Z_i T_i}} \quad (2.8)$$

Accurate calibration of all component volumes, in our case  $V_{ref}$ ,  $V_{bol}$  and  $V_{cold}$  gives our values for  $V_i$ . The temperatures of these volumes,  $T_{ref}$ ,  $T_{bol}$  and  $T_{cold}$  are measured using thermocouples or platinum thermometers. The compressibilities  $Z_i$  are functions of temperature and pressure i.e.  $Z_i(T_i, P_i)$  and  $P_{reference}$  and  $P_{sample}$  are also accurately measured. For an ideal gas  $Z_i = 1$  always. At the temperatures and pressures typical of the experimental conditions for this study (from vacuum to 700 bar pressure and room temperature to 300°C) hydrogen does not behave as an ideal gas and the  $Z_i$ 's must be accurately calculated.

This is a drawback of the Sieverts technique and a significant effort was required to find a reasonably convenient way of determining  $Z$  for both hydrogen and deuterium in the experimental conditions used in this study.

### 2.5.3 The Compressibility of Deuterium

For hydrogen and deuterium several analytic methods have been proposed to calculate the compressibility of hydrogen [5-8]. These three methods all fit a polynomial of some description to available data of the compressibility of hydrogen and/or deuterium.

A more accurate, though clumsier, method was presented by Hemmes *et al* [9]. This method uses a modified van der Waals equation

$$\left( P + \frac{a(P)}{V^\alpha} \right) (V - b(P)) = RT \quad (2.9)$$

where  $b(P)$  is a pressure dependent excluded volume,  $a(P)$  a pressure dependent interaction term and  $\alpha$  is approximately constant (but not equal to two as in the usual van der Waals equation)

$$a(P) = \exp(a_1 + a_2 \ln(P) - \exp(a_3 + a_4 \ln(P))) \quad (P > 1 \text{ bar}) \quad (2.10)$$

$$b(P) = \begin{cases} \sum_{i=0}^8 b_i \ln(P)^i & (P \geq 100 \text{ bar}) \\ b(100) & (P < 100 \text{ bar}) \end{cases} \quad (2.11)$$

$$\alpha(T) = \alpha_0 + \alpha_1 T + \alpha_2 T^2 \quad (2.12)$$

Table 2.1 gives the values for the coefficients for protium in the above equations. Since these equations attempt to model the physics behind the non-ideal behaviour of hydrogen, its accuracy extends over a wider range of temperatures and pressures than the other methods mentioned above. The inconvenience of Hemmes equation is that it must be solved numerically, a small price to pay considering the ready availability of Windows-based computation packages.

The coefficients in equations 2.10, 2.11 and 2.12 are all unit-less. The coefficients of Table 2.1 can only be used with units of temperature in Kelvin, volume in cc and pressure in bar. They do not scale with a change of unit, but must be refitted. Another way of saying the same is that equation 2.9 uses normalized values of  $P$ ,  $T$  and  $V$  (i.e.  $P$  is actually  $P/P_0$  where  $P_0 = 1$  bar). Coefficients in the equations reported in [5-9] are quoted without units for this reason.

The same comments can be applied to equations (2.13 – 2.16) and the coefficients of Table 2.2

**Table 2.1.** Hydrogen: Coefficients determining  $a$ ,  $b$  and  $\alpha$  in equations (2.10)-(2.12)

$\alpha_0$	2.9315	$a_1$	19.599
$\alpha_1$	$-1.531 \times 10^{-3}$	$a_2$	-0.8946
$\alpha_2$	$4.154 \times 10^{-6}$	$a_3$	-18.608
		$a_4$	2.6013
$b_0$	20.285	$b_5$	-0.12385414
$b_1$	-7.44171	$b_6$	$9.8570583 \times 10^{-3}$
$b_2$	7.318565	$b_7$	$-4.1153723 \times 10^{-4}$
$b_3$	-3.463717	$b_8$	$7.02499 \times 10^{-6}$
$b_4$	0.87372903		

A similar equation was developed for deuterium using the available experimental data [10], which was less than the data available to Hemmes for hydrogen. This was accomplished using the Windows based Mathematica package. Several approaches were taken to find the most accurate form of Hemmes equation, and the best result is described in [10] along with a comparison of its results against those obtained from the equation of states described in [6] and [8]. The equation for deuterium is then

$$\left( P + \frac{a(P)}{V^\alpha} \right) (V - b(P)) = RT \quad (2.13)$$

$$a(P) = \exp(a_1 + a_2 \ln(P) - \exp(a_3 + a_4 \ln(P))) \quad (P > 1 \text{ bar}) \quad (2.14)$$

$$b(P) = \begin{cases} \sum_{i=0}^8 b_i \ln(P)^i & (P \geq 100\text{bar}) \\ b(100) & (P < 100\text{bar}) \end{cases} \quad (2.15)$$

$$\alpha(T) = \alpha_0 + \alpha_1 T + \alpha_2 T^2 \quad (2.16)$$

The values for the constants for deuterium are shown in Table 2.2.

**Table 2.2.** Deuterium: Coefficients determining  $a$ ,  $b$  and  $\alpha$  in equations (2.13)-(2.15)

$\alpha_0$	2.75133	$a_1$	18.76040
$\alpha_1$	$-6.21145 \times 10^{-5}$	$a_2$	-0.74606
$\alpha_2$	$4.37677 \times 10^{-7}$	$a_3$	-8.69181
		$a_4$	$-1.03114 \times 10^{-3}$
$b_0$	20.285	$b_5$	-0.12385414
$b_1$	-7.44171	$b_6$	$9.8570583 \times 10^{-3}$
$b_2$	7.318565	$b_7$	$-4.1153723 \times 10^{-4}$
$b_3$	-3.463717	$b_8$	$7.02499 \times 10^{-6}$
$b_4$	0.87372903		

#### 2.5.4 Hot-Cold Volume Model

When a sample volume is partially located in a furnace or cryostat, that volume will have two zones at different temperatures. In a method developed by Gray [11] a model is made of this situation that allows the volume of these zones to be calculated

A volume of gas is at two differing temperatures, partly immersed say, in a furnace or cryostat. We will assume a sharp boundary between the regions of the differing temperatures. We have

$$V_{\text{sys}} = V_{\text{ref}} + V_{\text{samp}} \quad (2.17)$$

There is a fixed amount of gas  $n_0$  in  $V_{\text{sys}}$  to start with

$$n_0 = \frac{P_0}{R} \left\{ \frac{V_{ref}}{T_{ref}^0} + \frac{V_{samp}}{T_{samp}^0} \right\} \quad (2.18)$$

and the sample space is initially isothermal.

With part of  $V_{samp}$  at a higher temperature

$$n_0 = \frac{P}{R} (T_{samp}) \left\{ \frac{V_{ref}}{T_{ref}} + \frac{V_{cold}}{T_{samp}^0} + \frac{V_{hot}}{T_{samp}} \right\} \quad (2.19)$$

$$\begin{aligned} P_0 \left\{ \frac{V_{ref}}{T_{ref}^0} + \frac{V_{samp}}{T_{samp}^0} \right\} &= P(T_{samp}) \left\{ \frac{V_{ref}}{T_{ref}} + \frac{V_{cold}}{T_{samp}^0} + \frac{V_{hot}}{T_{samp}} \right\} \\ \frac{P_0}{P(T_{samp})} \left\{ \frac{V_{ref}}{T_{ref}^0} + \frac{V_{samp}}{T_{samp}^0} \right\} &= \frac{V_{ref}}{T_{ref}} + \frac{V_{cold}}{T_{samp}^0} + \frac{V_{hot}}{T_{samp}} \\ \frac{P_0}{P(T_{samp})} \left\{ \frac{V_{ref}}{T_{ref}^0} + \frac{V_{samp}}{T_{samp}^0} \right\} - \frac{V_{ref}}{T_{ref}} &= \frac{V_{cold}}{T_{samp}^0} + \frac{V_{hot}}{T_{samp}} \end{aligned} \quad (2.20)$$

By plotting the left-hand-side against  $1/T_{samp}$  a straight line with slope  $V_{hot}$  and y-intercept  $V_{cold}/T_{samp}^0$  is obtained.

## 2.6 Neutron-Beam Diffraction Instruments.

Three different neutron-beam diffraction instruments, using both fixed wavelength and time-of-flight (TOF) back-scattering principles, were used throughout this study.

The principle fixed-wavelength instruments used were the Medium Resolution neutron Powder Diffractometer (MRPD) and the High Resolution neutron Powder Diffractometer (HRPD) both located on the High Flux Australian Reactor (HIFAR) at the Australian National Science and Technology Organisation (ANSTO) facilities at Lucas Height, Sydney Australia. Results from the High Resolution Powder Diffractometer – thermal neutrons (HRPT) at the SINQ spallation source, Paul Scherrer Institute, Villigen, Switzerland were also used.

The instrument used for TOF studies was the High Resolution neutron Powder Diffractometer (HRPD) at the ISIS neutron spallation source, Rutherford Appleton Laboratories (RAL) in Oxfordshire, U.K

Protium scatters neutrons incoherently, and so is useless if hydrogen crystallographic location information is sought from neutron-diffraction experiments. Deuterium has a neutron scattering length of 6.671 fm, very similar to palladium at 5.91 fm, so its influence on the palladium lattice is easy to detect. Deuterium gas is therefore used in all of the neutron scattering experiments here.

### **2.6.1 The HIFAR MRPD Instrument**

The MRPD instrument at HIFAR can be used in either high intensity or high resolution mode by varying the primary collimator setting to either  $0.25^\circ$  or  $0.45^\circ$ . To further improve the flux, MRPD uses a vertically focusing Ge monochromator with  $2\theta_M=100^\circ$  take off angle situated 1.9 m from the reactor face. Wavelengths can be selected in the range 1.06 - 4.99 Å. The flux at the sample position is  $3.8 \times 10^5 \text{ ncm}^{-2}\text{s}^{-1}$  in high intensity mode, and  $2.1 \times 10^5 \text{ ncm}^{-2}\text{s}^{-1}$  in high resolution mode. MRPD currently has 32  $\text{He}^3$  detectors separated by  $4^\circ$ , with individual collimation yielding an acceptance angle of  $0.35^\circ$ . The detector bank  $2\theta$  range is  $4^\circ$  to  $138^\circ$  in  $0.1^\circ$  steps. The instrumental peak-width on MRPD is roughly double that on the HIFAR HRPD instrument (see Section 2.4.2), though it gains a factor of approximately 6.3 in speed. Given its useful collection of ancillary equipment (furnaces, cryo-refrigerators, high-intensity magnets), MRPD's instrumental setup is excellent for studying in-situ phase transitions.

### **2.6.2 The HIFAR HRPD instrument**

HRPD has a  $2\theta_M=120^\circ$  monochromator take-off angle, providing a minimum in profile resolution at  $2\theta \sim 120^\circ$  in the diffraction pattern. The primary thermal flux of  $1.4 \times 10^{14} \text{ ncm}^{-2}\text{s}^{-1}$  hits a 20 cm long primary beam collimator that reduces the horizontal divergence to  $0.25^\circ$  before reaching the Ge monochromator at a distance of 2.25 m from the reactor face. The monochromator is constructed of eight squashed Ge crystals with a mosaic spread of  $0.2^\circ$ . Wavelengths are selectable in the range 1.20 - 5.66 Å. After reflection through the monochromator, the beam travels 1.2 m to the sample position through a 20 mm  $\times$  50 mm guide. The flux at the sample position depends upon the selected



wavelength, with a peak at  $1.88 \text{ \AA}$  of  $8 \times 10^4 \text{ ncm}^{-2}\text{s}^{-1}$ . The instrument has 24  $\text{He}^3$  detectors separated by  $4^\circ$ . The detector bank has individual collimation on each detector yielding a parallel configuration with horizontal divergence  $0.17^\circ$ , removing sample dependent divergence. The entire detector bank  $2\theta$  range is  $5^\circ$  to  $155^\circ$  in  $0.05^\circ$  steps. HRPD also has a range of ancillary equipment for altering sample conditions.

A photograph of the HRPD diffractometer is shown in Fig 2.5

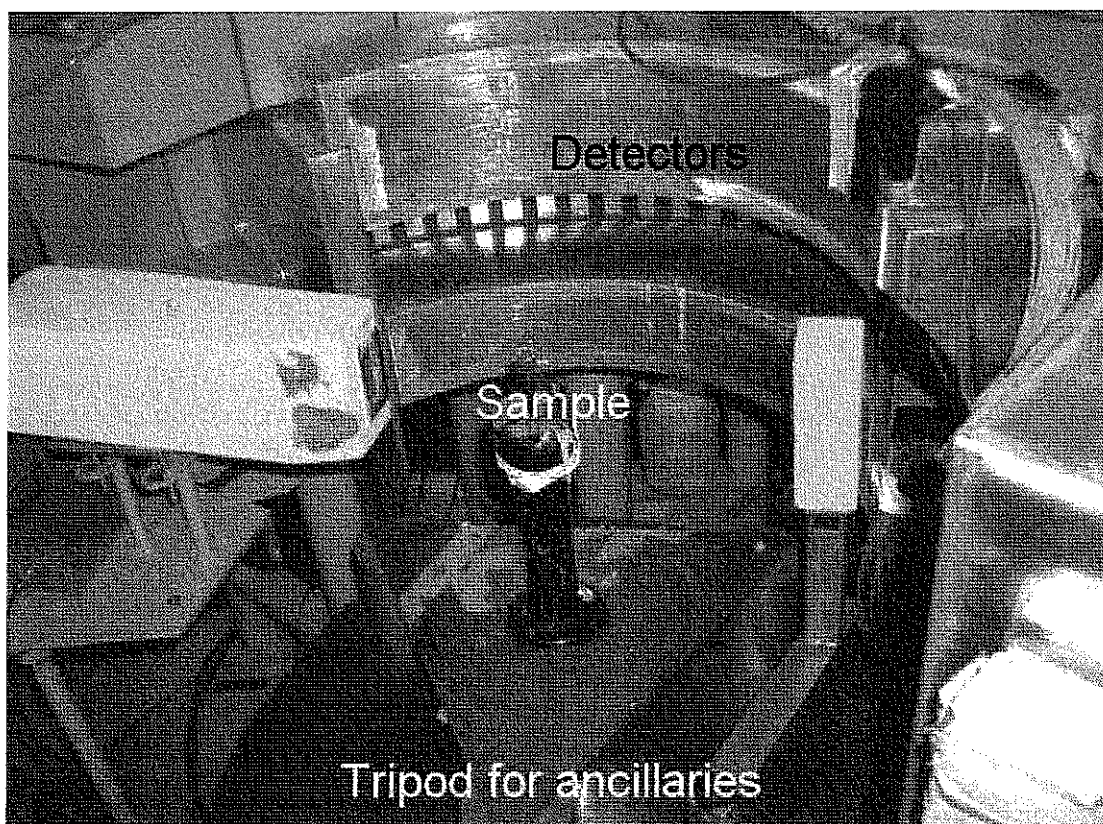


Fig 2.5 The HRPD diffractometer on beam line 4H1 of HIFAR

### 2.6.3 The SINQ HRPT Instrument

The multi-detector diffractometer HRPT is designed as a flexible instrument for efficient neutron powder diffraction studies, especially for small sample sizes. High resolution is achieved by thermal neutrons, large scattering angles of the monochromator and of the sample (up to  $165^\circ$ ). Primary collimators, a secondary slit system and appropriate choice of the sample diameter optimise resolution and intensity. Due to the use of a large position sensitive (PSD)  $^3\text{He}$  detector, simultaneous measurements are possible within a scattering angle range of 160 degrees with angular steps  $0.1^\circ$ . Depending on the desired point density and resolution up to  $\delta d/d < 0.002$  in high intensity mode, and  $\delta d/d < 0.001$  in high resolution mode may be obtained (take-off-angle  $2\theta_M = 120^\circ$ ,  $d$  = interplanar spacing). The detector may also be positioned on air cushions for intermediate positions. Standard measurements are performed by means of an evacuated aluminium pot equipped with a cooling machine, which can be oscillated to reduce preferred orientation effects of the sample. An oscillating radial collimator suppresses Bragg peaks from the sample environment such as cryostats or furnaces.

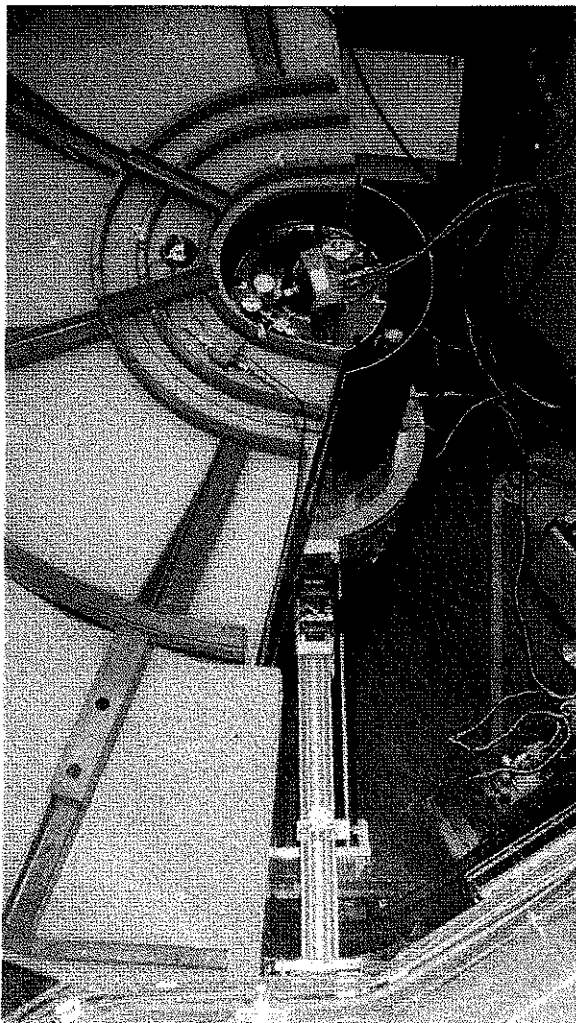


Fig 2.6: View of the sample table on HRPT, SINQ spallation source at PSI, Switzerland.

Fig 2.6 shows a photograph of the sample table of HRPT. Fig 2.7 illustrates the

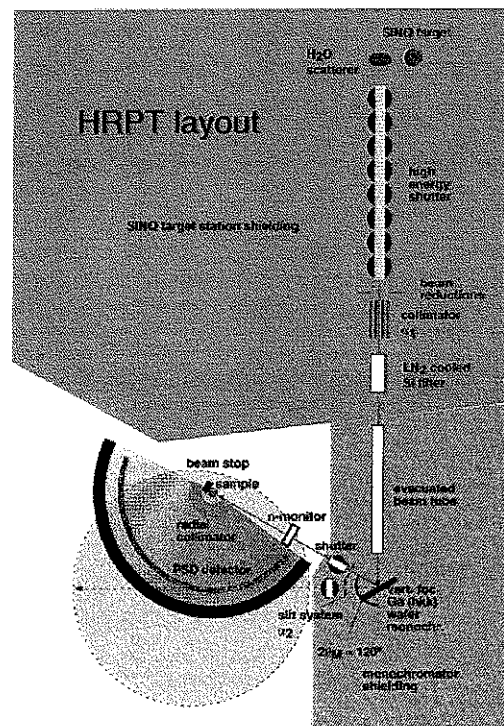


Fig 2.7: Schematic diagram of the SINQ HRPT instrument setup

2.4 is also a photograph of the SINQ HRPT instrument

#### 2.6.4 The ISIS HRPD Instrument

HRPD is the highest resolution neutron-beam diffractometer in the world. In back-scattering it displays an essentially constant  $\Delta d/d \sim 4 \times 10^{-4}$  across the entire d-spacing range available on the instrument. The high resolution is obtained by placing the diffractometer at a large distance from the moderator, introducing a longer neutron flight path and increasing both denominators in the resolution expression

$$R(d) = \frac{\Delta d}{d} = \left\{ \Delta \theta^2 \cot^2 \theta + \left( \frac{\Delta t}{t} \right)^2 + \left( \frac{\Delta L}{L} \right)^2 \right\}^{\frac{1}{2}} \quad (2.21)$$

The  $\Delta \theta \cot \theta$  product is reduced the most at large scattering angles

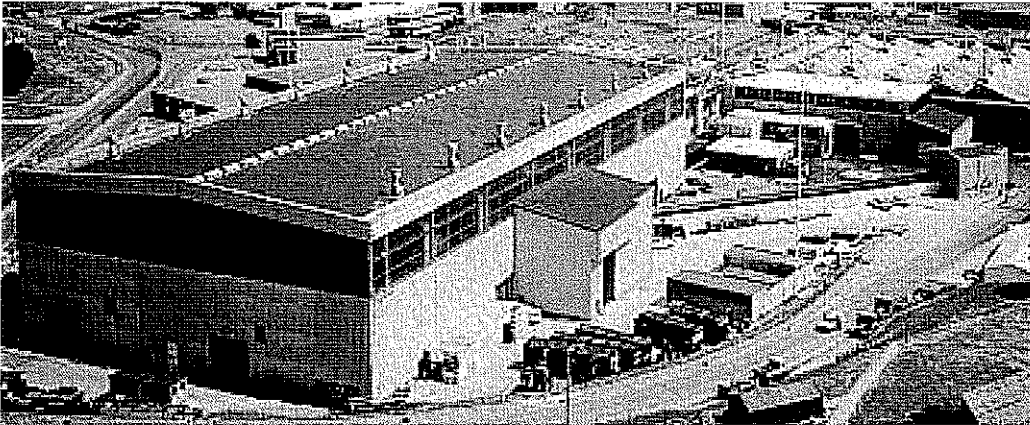


Fig 2.8 ISIS facility at RAL, Oxfordshire UK. The spallation source and majority of instruments are located in the large building at left. The HRPD instrument is located in the small brick building to the right of the picture, at the end of a race covering the beam-line.

Neutrons are guided from the moderator through a curved Ni plated glass guide tube to avoid line-of-sight fast neutrons. Choppers at 6 m and 9 m eliminate frame overlap where the fast end of the subsequent pulse overlaps the slow end of the leading pulse. The sample position at 96 m yields the highest resolution. Octant configuration ZnS back scattering scintillator detectors minimize geometric aberration by following the diffracted Debye-Scherrer cone profile. As the angular range subtended is quite small, any wavelength dependent attenuation of neutrons is effectively removed, allowing study of strongly

attenuating samples up to 20 mm in radius without the need for complicated attenuation correction routines.

## 2.7 Density Functional Theory

Computational analysis of the palladium-hydride system was carried out by *density functional theory* (DFT) calculations using the Amsterdam Density Functional (ADF) software suite, explicitly the BAND sub-suite of programs, which are used to perform calculations on periodic structures in one-, two- or three-dimensions (i.e. polymers, slabs and bulk-solids). All further discussion of theory and results of the computational study done in this thesis appear in Chapter 6

1. Wicke, E. and H. Brodowsky, *Hydrogen in Palladium and Palladium Alloys*, in *Hydrogen in Metals II. Application-Oriented Properties*, G. Alefeld and J. Volkl, Editors 1978, Springer-Verlag: Berlin p 81
2. Wicke, E. and B. J., *New Experiments on and Interpretations of Hysteresis Effects of Pd-D<sub>2</sub> and Pd-H<sub>2</sub>*, Journal of the Less-Common Metals, 1987 **130**: p. 351-363.
3. Fukai, *Hydrogen in Metals*.
4. Bennington, S.M., et al., *In-situ Measurements of Deuterium Uptake into a Palladium Electrode Using Time-of-Flight Neutron Diffractometry*, Journal of Electroanalytic Chemistry, 1990. **281**: p. 323-330.
5. Michels, A., et al., *Compressibility isotherms of hydrogen and deuterium at temperatures between -175°C and +150°C (at densities up to 960 amagat)*, Physica, 1959 **25**: p. 25-42.
6. Mills, R.L., et al., *Equation of state of fluid n-H<sub>2</sub> from P-V-T and sound velocity measurements to 20 kbar*, The Journal of Chemical Physics, 1977. **66**(7): p. 3076-3084
7. Mills, R.L., D.H. Liebenberg, and J.C. Bronson, *Equation of state of fluid n-D<sub>2</sub> from P-V-T and sound velocity measurements to 20 kbar*, The Journal of Chemical Physics, 1978 **68**: p. 2663.
8. Tkacz, M. and A. Litwiniuk, *Useful equations of state of hydrogen and deuterium*, Journal of Alloys and Compounds, 2002. **330-332**: p. 89-92
9. Hemmes, H., A. Driessen, and R. Griessen, *Thermodynamic properties of hydrogen at pressures up to 1 Mbar and temperatures between 100 and 1000K*, Journal of Physics C: Solid State Physics, 1986 **19**: p. 3571-3585.
10. McLennan, K.G. and E.M. Gray, *An equation of state for deuterium gas to 1000 bar*, Measurement Science and Technology, 2004. **15**: p. 211-215
11. Gray, E.M., *A Hot-Cold Volume Model*, K.G. McLennan, Editor. 2000: Brisbane